Two-Electron Interference in Strong-Field Ionization of He by a Short Intense Extreme Ultraviolet Laser Pulse

Wei-Chao Jiang,[1,2,3,*] Si-Ge Chen,[2] Liang-You Peng,[2,4,†] and Joachim Burgdörfer[3]
[1]College of Physics and Optoelectronic Engineering, Shenzhen University, Shenzhen 518060, China
[2]State Key Laboratory for Mesoscopic Physics and Collaborative Innovation Center of Quantum Matter, School of Physics, Peking University, Beijing 100871, China
[3]Institute for Theoretical Physics, Vienna University of Technology, Wiedner Hauptstraße 8-10, A-1040 Vienna, Austria, EU
[4]Beijing Academy of Quantum Information Sciences, Beijing 100193, China

(Received 19 March 2019; published 30 January 2020)

Double ionization of helium by a single intense (above 10^{18} W/cm^2) linearly polarized extreme ultraviolet laser pulse is studied by numerically solving the full-dimensional time-dependent Schrödinger equation. For the laser intensities well beyond the perturbative limit, novel gridlike interference fringes are found in the correlated energy spectrum of the two photoelectrons. The interference can be traced to the multitude of two-electron wave packets emitted at different ionization times. A semianalytical model for the dressed two-photon double ionization is shown to qualitatively account for the interference patterns in the joint energy spectrum. Similar signatures of interferences between transient induced time-delayed ionization bursts are expected for other atomic and molecular multielectron systems.

DOI: 10.1103/PhysRevLett.124.043203

Recent developments in free-electron laser technologies [1–11] promise to provide strong extreme ultraviolet (XUV) lasers pulses with peak intensities reaching 10^{18} W/cm^2, which opens the door to study novel nonperturbative interactions between atoms and light fields complementally to the well-explored near-adiabatic Keldysh regime $\omega \ll I_p$ accessible by strong-field infrared (IR) or midinfrared (MIR) pulses [12]. The interplay between strong-field effects and electron correlations has been experimentally investigated for IR pulses [13–15]. Distinct nonsequential double-ionization processes have been identified, such as the recollision ionization [15] and the recollision-induced excitation of the ion plus subsequent field ionization (RESI) [16,17]. In the XUV regime, however, most previous studies of double ionization focused on the perturbative regime, in particular on the one-photon [18–22] and two-photon [23–41] double ionization. Effects beyond the lowest-order perturbation theory such as the ac Stark shifts [42] in the joint energy spectra for double ionization of helium by intense XUV pulses were studied by solving the reduced-dimension time-dependent Schrödinger equation (TDSE).

In this Letter, we report on multielectron emission and interferences in the strong-field high-frequency regime. Multiparticle interferences controlled by fermionic or bosonic quantum correlations are currently of considerable topical interests for a variety of systems (see, e.g., Ref. [43]). As a "simple" prototypical case, we study two-electron interferences in the double ionization of helium by a single strong XUV laser pulse in the nonperturbative regime, for which a numerically accurate solution of the many-electron TDSE in its full dimensionality is still feasible. Significant population on the single continuum with the bound electron on the $1s$ state of He^+ and the exchange symmetry of the entangled electrons in the singlet sector are found to be key ingredients for the appearance of these dynamic multi-electron interferences.

For one-electron emission by strong-field XUV pulses, prominent dynamic interference features have been previously identified [44–51]. Accordingly, the ejection of electrons takes place at different points in time within the envelope of a single pulse featuring the same ac Stark shift [44–51] giving rise to phase differences between the two ensuing wave packets. Such time interferences originating within a single pulse complement those that occur from a more conventional pump-probe sequence where wave packets are ejected by either the pump or the probe pulse accumulating a phase difference depending on the time delay between the pump and the probe [52–54]. The dynamic interference in the single ionization of atoms leads to the surprising modulation of the photoelectron spectrum (PES) ("peak splitting"). This modulation bears resemblance to fine structures experimentally observed in the above threshold ionization (ATI) by a strong pulse with $\omega \ll I_p$ [55–57]. The underlying process is, however, fundamentally different. The peak splitting in the ATI is caused by so-called Freeman resonances of highly excited states that are ac Stark shifted into resonance as intermediate states along the multiphoton pathway to the continuum [55–57]. Dynamic interference in the high-frequency ($\omega > I_p$) strong-field regime, by contrast, does not involve intermediate state resonances but, instead, a time-double slit of two sequential ionization bursts,

one on the rising flank and the other on the falling flank of the envelope of the ultrashort XUV pulse.

As demonstrated for one-electron or single active electron (SAE) models [51], the rapid depletion of the population of the initial state on the rising edge hampers the appearance of these interferences as it tends to shut down one of the two "arms" of the interferometer. The point of departure of the present study is that for multielectron emission in many-electron systems the proliferation of interfering pathways may facilitate the appearance of such dynamic interferences. For the present case of helium, the two-electron wave packets ejected in the double ionization feature additional interfering paths originating from the time delayed emission and the exchange symmetry of the two electrons (Fig. 1). The double continuum states $|\mathbf{k}_1, \mathbf{k}_2\rangle$ can be reached either by double ejection on the rising edge (paths $R1$ and $R2$) of the pulse or by double ejection on the falling edge (paths $F1$ and $F2$) or by ejection of an electron from the neutral ground state on the rising edge and the subsequent time-delayed (td) emission of the other electron from the ground state of He^+ on the falling edge (paths $F1$td and $F2$td). Electron ejection from the neutral ground state occurs primarily on the rising edge due to the near-complete depletion except for the shortest pulses, but the electron from He^+ can be ejected on either the rising or the falling edge of the laser pulse. Transient strong-field stabilization in the high-frequency field, i.e., suppression of the photoelectric effect [58], here operational primarily for the He^+ ion, plays a crucial role

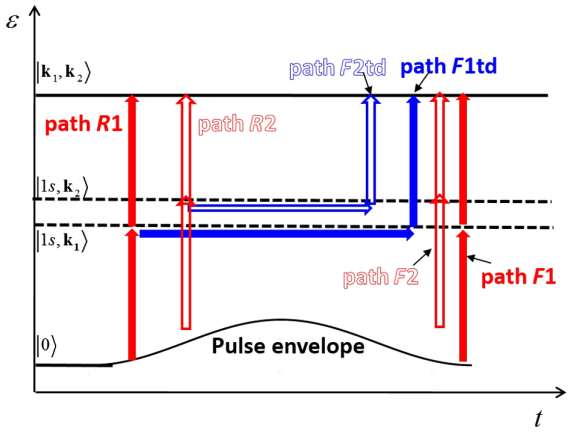

FIG. 1. Schematic path interferences for two-photon emission by a single strong XUV pulse with envelope $F_0(t)$ and temporal width of the order of ~fs. Double ionization can take place either with the emission of both electrons on the rising (R) edge of the pulses (paths $R1$ and $R2$) or on the falling (F) edge (paths $F1$ and $F2$) or with the emission of the first electron on the rising edge and the time-delayed emission of the second electron on the falling flank (paths $F1$td and $F2$td). Double emission on the falling flank ($F1$ and $F2$) is suppressed due to the rapid depletion of the neutral ground state except for the shortest pulses. The paths (2) are exchange-symmetric counterparts to the paths (1). The localization of the ionization time results from the strong ac Stark shift controlled by the envelope $F_0(t)$.

preventing the complete depletion of the ionic ground state before reaching the falling edge of the pulse [44,59].

Our numerical approach for solving the full-dimensional TDSE is based on the close-coupling expansion, the finite-element discrete variable representation (FE-DVR) method [60–62], and the Lanczos propagation algorithm [63,64]. The velocity gauge is chosen to describe the electron-laser interaction Hamiltonian since much fewer partial waves are required in the velocity gauge than that in the length gauge [51,65–67] to reach converged results. Typically, the single-electron angular momentum number l_1 (l_2) is taken up to 8 and the total angular momentum number L up to 4. Convergence has been ensured by varying the number of included partial waves. The maximal box size for the radial coordinates is chosen to be 400 a.u., and an absorbing mask function has been applied in each step of time propagation of the wave function. We choose XUV pulses with envelope of $\sin^2$ shape.

In Fig. 2, we present results for the variation of the joint energy spectra with key parameters of the strong and ultrashort XUV pulse. The first row displays the dependence on the peak intensity $I = F_0^2$, the second on photon energy ω, and the third on the pulse duration T_p. The intensity dependence (a1–a3) covers the range from the low-intensity

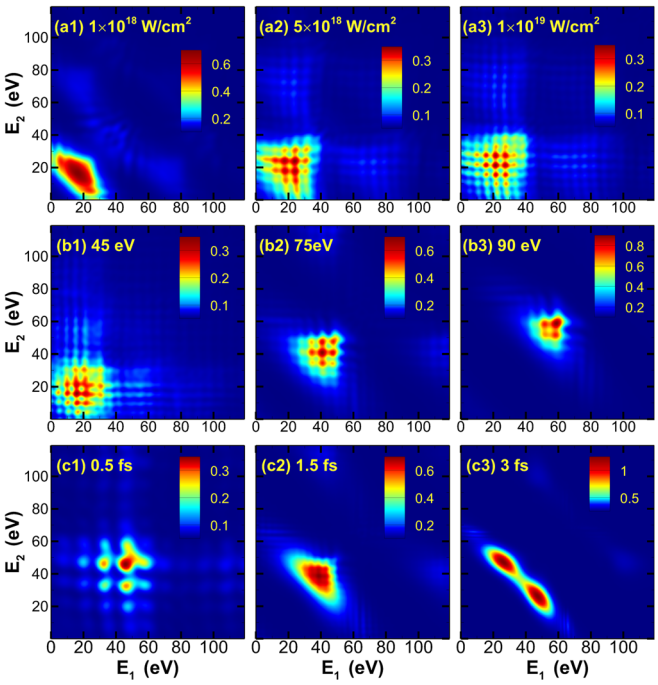

FIG. 2. Joint photoelectron energy spectra for double ionization of helium from full-dimensional TDSE calculations. First row (a): variation with peak intensity as indicated at fixed photon energy (54.6 eV) and the pulse duration (1 fs). Second row (b): variation with photon energy at fixed peak intensity (1×10^{19} W/cm^2) and the pulse duration (1 fs). Third row (c): variation with pulse duration at fixed peak intensity (1×10^{19} W/cm^2) and photon energy (75 eV).

double ionization where the two-photon ionization dynamic interference is absent (a1) to the strong-field regime (a3) featuring a pronounced Cartesian gridlike dynamic interference pattern in the $E_1 - E_2$ plane with a grid spacing $\Delta E_1 = \Delta E_2 \approx 5$ eV given by $\Delta E_1 = 2\pi/\Delta T$ with ΔT the effective time delay between the ionization bursts on the rising and falling flank (Fig. 1). The dependence on photon energy (b1–b3) indicates that dressed two-photon double ionization strongly dominates over one-photon double ionization events even when one-photon ionization is energetically permitted for $\omega > I_{p2}$ (b3, the double ionization potential I_{p2} of He is 79.01 eV). This observation highlights the strongly nonperturbative character of double ionization in this intensity regime. Finally, the dependence on pulse duration (c1–c3) reveals the fact that ultrashort pulses are key to observe pronounced dynamical interferences (c1). For long pulses exceeding a few femtoseconds, the dynamical interference patterns disappear (c3) as eventually the depletion of the ionic state [$He^+(1s)$] closes the corresponding interference channel (see Fig. 1). The resulting joint energy spectra shown in Fig. 2 are dominated by two-photon absorption processes, leading to a dominant signal near the line $E_1 + E_2 = 2\omega - I_{p2}$. At higher intensities [see, e.g., frame (a3)], weak traces of the three-photon double ionization signal near $E_1 + E_2 = 3\omega - I_p$ appear which mirror the grid structure.

In order to trace the origin of the interference pattern and to identify the contributing paths we analyze the results of the full TDSE calculation in terms of a simplified semianalytical model that resembles, to some extent, the virtual-sequential model for two-photon ionization of helium [29–34], and employs Coulomb-Volkov states [68]. Even though explicitly treating only two-photon absorption, it nevertheless can account for the dressing by nonperturbative high-order corrections and for the depletion of the initial state and strong-field distortion of the final state. Accordingly, we decompose the double ionization process into a virtual sequence of two one-photon absorption events. The differential change in ionization amplitude during the absorption of the first photon ($P1$) can be expressed as (atomic units are used unless otherwise stated)

$$da^{P1}_{\mathbf{k}_1} = -\langle \psi_{\mathbf{k}_1,1s}| \frac{\partial}{\partial z_1} + \frac{\partial}{\partial z_2} |\psi_0\rangle a_0(\tau_1) A(\tau_1) d\tau_1, \quad (1)$$

where ψ_0 and $\psi_{\mathbf{k}_1,1s}$ are the neutral ground state and the single ionization continuum state of helium, respectively, coupled by the dipole matrix element, $a_0(\tau_1)$ is the occupation amplitude of the ground state which is allowed to vary when the depletion and ac Stark shifts are taken into account, and $A(\tau_1)$ is the vector potential of the laser pulse with polarization direction along the z axis. The final state of the photoionized electron is described by a Coulomb-Volkov state with the Volkov phase

$$\Phi_{\mathbf{k}_1}(t_f, \tau_1) = \int_{\tau_1}^{t_f} \left[\frac{k_1^2}{2} + k_{z1} A(\tau') \right] d\tau', \quad (2)$$

accumulated between the emission time τ_1 and the conclusion of the pulse at t_f. Analogously, the amplitude for the subsequent second photoabsorption event ($P2$) is given by

$$a^{P2}_{\mathbf{k}_2}(t_f, \tau_1) = -\langle \psi_{\mathbf{k}_2}| \frac{\partial}{\partial z} |\psi_{1s}\rangle \times \int_{\tau_1}^{t_f} a_{1s}(\tau_2, \tau_1) A(\tau_2) \exp[-i\Phi_{\mathbf{k}_2}(t_f, \tau_2)] d\tau_2, \quad (3)$$

where ψ_{1s} and $\psi_{\mathbf{k}_2}$ are the ground state and continuum state of He^+, respectively, and $a_{1s}(\tau_2, \tau_1)$ is the amplitude of the ground state of He^+ at time τ_2 when He^+ is exposed into the laser field at time τ_1.

Combining now the two ionization steps, we obtain the amplitude of the double ionization as

$$a^{D}_{\mathbf{k}_1,\mathbf{k}_2}(t_f, t_0) = \langle \psi_{\mathbf{k}_1,1s}| \frac{\partial}{\partial z_1} + \frac{\partial}{\partial z_2} |\psi_0\rangle \langle \psi_{\mathbf{k}_2}| \frac{\partial}{\partial z} |\psi_{1s}\rangle \times \int_{t_0}^{t_f} a_0(\tau_1) A(\tau_1) \exp[-i\Phi_{\mathbf{k}_1}(t_f, \tau_1)] \int_{\tau_1}^{t_f} a_{1s}(\tau_2, \tau_1) A(\tau_2) \exp[-i\Phi_{\mathbf{k}_2}(t_f, \tau_2)] d\tau_2 d\tau_1 + \mathbf{k}_1 \leftrightarrow \mathbf{k}_2, \quad (4)$$

which is referred to in the following as the strong-field dressed two-photon double ionization (SFD-TPDI) model. In the limit of low intensities, the SFD-TPDI model reduces to second-order perturbation theory for two-photon double ionization. Since the two electrons are initially in the antisymmetric and maximally entangled spin singlet state, $(1/\sqrt{2})(|\uparrow\downarrow\rangle - |\downarrow\uparrow\rangle)$, which is preserved during the interaction with the XUV pulse, the double ionization amplitude in the orbital degrees of freedom [Eq. (4)] is even under $(\mathbf{k}_1 \leftrightarrow \mathbf{k}_2)$ and the two exchange-symmetric partial amplitudes add up coherently. Details for the evaluation of the dipole transition matrix elements were discussed in previous studies [29–34,40].

Time-dependent amplitudes for the ground-state occupation $a_0(\tau_1)$ and the single ionization $a_{1s}(\tau_1, \tau_2)$ entering Eq. (4) can be obtained by independent calculations, e.g., using the perturbation theory [51] or the high-frequency Floquet theory (HFFT) [69] for the dynamical Stark shift

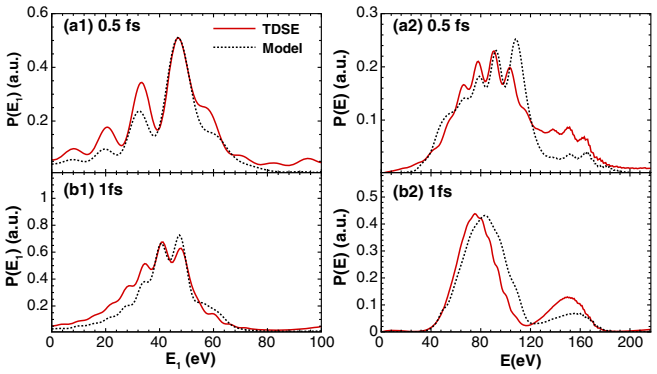

FIG. 3. Left column (a1, b1): one-electron spectrum $P(E_1)$ resulting from the integration over the energy E_2 of the second electron of the joint distribution $P(E_1, E_2)$; Right column (a2, b2): total energy spectrum $P(E)$ of the two-electron wave packet ($E = E_1 + E_2$). The pulse duration is taken to be 0.5 fs (top row: a1, a2) and 1 fs (bottom row: b1, b2). The photon energy is 75 eV, and the laser intensity is 1×10^{19} W/cm^2. The results from the SFD-TPDI model [Eq. (4)] are normalized to match the TDSE results.

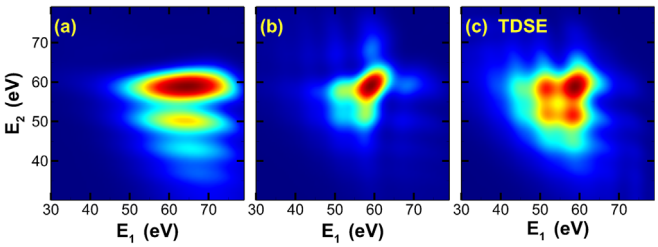

FIG. 4. Different levels of approximation to the joint energy distribution: (a) SFD-TPDI model [Eq. (4)] with exchange-symmetric term omitted, (b) SFD-TPDI model with exchange-symmetric term included, and (c) full TDSE calculation. The photon energy is 90 eV, the pulse duration is 1 fs, and the pulse intensity is 1×10^{19} W/cm^2.

and decay rate. In the present implementation of the model we extract these amplitudes directly from the solution of the TDSE (see Supplemental Material [59]). Overall, the SFD-TPDI model reproduces the interference patterns seen in the TDSE solutions quite well (Fig. 3). For a quantitative comparison, we calculate both the one-electron spectra determined by integration of the energy distribution of the second electron $P(E_1) = \int_0^\infty P(E_1, E_2) dE_2$ and the total two-electron energy spectra $P(E) = \int P(E_1, E - E_1) dE_1$. Though obvious discrepancies exist, the interference peaks from the model and the TDSE agree reasonably well with each other. The peak distance decreases as the pulse duration increases, reflecting the fact that the time delay between the ionization bursts becomes larger by lengthening the pulse. A broad peak around $E = 71$ eV corresponding energetically to two-photon absorption and a weaker peak around $E = 146$ eV corresponding to three-photon absorption can be clearly identified in the total two-electron energy spectra $P(E)$ [see Fig. 3(b2)]. The peak splitting, i.e., interference oscillations signifying dynamic interference between direct double ionization on the rising and on the falling flank of the pulse, become observable for ultrashort pulses $T_p = 0.5$ fs [Fig. 3(a2)]. For longer pulses $T_p = 1$ fs they are already strongly suppressed [Fig. 3(b2)]. This is due to the depletion of the neutral ground state ($|a_0(t)| < 0.01$ for longer pulses) precluding the interference between the double-electron ejection on the rising edge and the double-electron ejection on the falling edge. The effective closing of these two-electron ejection paths on the falling edge, however, does not remove the interference pattern in the one-electron spectra $P(E_1)$, as shown in Fig. 3(b1). For the latter, only a non-negligible amplitude of the ionic ground state at the falling edge is required. The multitude of pathways including those that involve different charge states renders dynamic interference in multielectron systems more robust than in effective one-electron systems.

The role of exchange symmetry can be identified by switching off the exchange-symmetric contribution [second term in Eq. (4)], as shown in Fig. 4. The joint distribution $P(E_1, E_2)$ is obviously now nonsymmetric, $P(E_1, E_2) \neq P(E_2, E_1)$. The interference stripes seen in Fig. 4(a) are due to the interference between paths $R1$ and $F1$td. Switching off, instead, the first term in Eq. (4) would give the mirrored stripes associated with the interferences between paths $R2$ and $F2$td. Adding all paths coherently [Fig. 4(b)] gives rise to a two-dimensional interference pattern qualitatively resembling the full TDSE result [Fig. 4(c)]. Differences are likely due to the neglect of dynamic electron-electron correlations in the model as well as the omission of an explicit treatment of third-(or higher) order photoabsorption processes in Eq. (4). Nevertheless, the model can reproduce the dominant interference structures shown in Fig. 2 (see Ref. [59] for more details).

In summary, we have performed the first fully *ab initio* study of double ionization of helium by ultrashort high-frequency XUV pulses with ω large compared to I_p in the strong-field regime. Sequential double ionization by two-photon absorption is found to be the dominant ionization channel, however significantly modified by nonperturbative strong-field effects. The two-photon double ionization process strongly dominates over the one-photon process even when the latter is energetically possible. Novel grid-like interference structures are identified in the joint energy spectrum of the two photoelectrons for intense and short XUV laser pulses. These dynamical two-electron interferences are considerably more robust against depletion of the initial state than the dynamic interference in single ionization. This is due to the presence of a multitude of interference pathways involving the sequential ionization on the rising and falling edge of the envelope of the XUV pulse including their exchange symmetric partners. The present dynamic interferences resulting from an interplay between ionization bursts temporally separated and proliferation of multielectron ionization paths are expected to be present also in other two-electron atoms, ions, or

molecules, e.g., H^- or H_2. More generally, interference effects involving multielectron emission facilitated by the transient suppression of the photoelectric effect may emerge in more complex atoms and molecules. Future experiments with intense XUV sources should allow for tests of the present predictions.

This work is supported by the National Natural Science Foundation of China (NSFC) (Grants No. 11804233 and No. 11725416), by the National Key R&D Program of China (Grant No. 2018YFA0306302), and by Grants No. FWF-SFB049 (Nextlite), No. FWF-SFB041 (VICOM), No. WWTF MA1FOR-002, Doctoral college Grant No. FWF-W1243 (Solids for Function).

*jiang.wei.chao@szu.edu.cn
†liangyou.peng@pku.edu.cn

[1] E. A. Seddon, J. A. Clarke, D. J. Dunning, C. Masciovecchio, C. J. Milne, F. Parmigiani, D. Rugg, J. C. H. Spence, N. R. Thompson, K. Ueda, S. M. Vinko, J. S. Wark, and W. Wurth, Rep. Prog. Phys. **80**, 115901 (2017).
[2] B. W. J. McNeil and N. R. Thompson, Nat. Photonics **4**, 814 (2010).
[3] S. Huang, Y. Ding, Y. Feng, E. Hemsing, Z. Huang, J. Krzywinski, A. A. Lutman, A. Marinelli, T. J. Maxwell, and D. Zhu, Phys. Rev. Lett. **119**, 154801 (2017).
[4] T. Ishikawa *et al.*, Nat. Photonics **6**, 540 (2012).
[5] E. Allaria, B. Diviacco, C. Callegari, P. Finetti, B. Mahieu, J. Viefhaus, M. Zangrando, G. DeNinno, G. Lambert *et al.*, Phys. Rev. X **4**, 041040 (2014).
[6] M. Altarelli, R. Brinkmann, M. Chergui, W. Decking, B. Dobson, S. Düsterer, G. Grübel, W. Graeff, H. Graafsma, J. Hajdu *et al.*, XFEL: The European X-ray free-electron laser, Technical design report, 2006, http://www-library.desy.de/cgi-bin/showprep.pl?desy06-097.
[7] M. Altarelli, Nucl. Instrum. Methods Phys. Res., Sect. B **269**, 2845 (2011).
[8] M. W. Guetg, A. A. Lutman, Y. Ding, T. J. Maxwell, F.-J. Decker, U. Bergmann, and Z. Huang, Phys. Rev. Lett. **120**, 014801 (2018).
[9] M. Fuchs *et al.*, Nat. Phys. **11**, 964 (2015).
[10] A. A. Sorokin, S. V. Bobashev, T. Feigl, K. Tiedtke, H. Wabnitz, and M. Richter, Phys. Rev. Lett. **99**, 213002 (2007).
[11] C. Ott *et al.*, Phys. Rev. Lett. **123**, 163201 (2019).
[12] H. R. Reiss, Phys. Rev. Lett. **101**, 043002 (2008).
[13] W. Becker, X. J. Liu, P. J. Ho, and J. H. Eberly, Rev. Mod. Phys. **84**, 1011 (2012).
[14] C. F. d. M. Faria and X. Liu, J. Mod. Opt. **58**, 1076 (2011).
[15] P. B. Corkum, Phys. Rev. Lett. **71**, 1994 (1993).
[16] Y. Liu, S. Tschuch, A. Rudenko, M. Durr, M. Siegel, U. Morgner, R. Moshammer, and J. Ullrich, Phys. Rev. Lett. **101**, 053001 (2008).
[17] R. Kopold, W. Becker, H. Rottke, and W. Sandner, Phys. Rev. Lett. **85**, 3781 (2000).
[18] M. S. Schöffler, C. Stuck, M. Waitz, F. Trinter, T. Jahnke, U. Lenz, M. Jones, A. Belkacem, A. L. Landers, M. S. Pindzola, C. L. Cocke, J. Colgan, A. Kheifets, I. Bray, H. Schmidt-Böcking, R. Dörner, and T. Weber, Phys. Rev. Lett. **111**, 013003 (2013).
[19] L. Avaldi and A. Huetz, J. Phys. B **38**, S861 (2005).
[20] A. Knapp, A. Kheifets, I. Bray, T. Weber, A. L. Landers, S. Schössler, T. Jahnke, J. Nickles, S. Kammer, O. Jagutzki, L. Ph. H. Schmidt, T. Osipov, J. Rösch, M. H. Prior, H. Schmidt-Böcking, C. L. Cocke, and R. Dörner, Phys. Rev. Lett. **89**, 033004 (2002).
[21] A. Huetz and J. Mazeau, Phys. Rev. Lett. **85**, 530 (2000).
[22] O. Schwarzkopf, B. Krässig, J. Elmiger, and V. Schmidt, Phys. Rev. Lett. **70**, 3008 (1993).
[23] S. X. Hu, Phys. Rev. A **97**, 013414 (2018).
[24] J. M. N. Djiokap and A. F. Starace, J. Opt. **19**, 124003 (2017).
[25] H. W. van der Hart, Phys. Rev. A **89**, 053407 (2014).
[26] J. Feist, S. Nagele, R. Pazourek, E. Persson, B. I. Schneider, L. A. Collins, and J. Burgdörfer, Phys. Rev. Lett. **103**, 063002 (2009).
[27] J. Colgan and M. S. Pindzola, Phys. Rev. Lett. **88**, 173002 (2002).
[28] E. Foumouo, G. L. Kamta, G. Edah, and B. Piraux, Phys. Rev. A **74**, 063409 (2006).
[29] D. A. Horner, F. Morales, T. N. Rescigno, F. Martín, and C. W. McCurdy, Phys. Rev. A **76**, 030701(R) (2007).
[30] D. A. Horner, C. W. McCurdy, and T. N. Rescigno, Phys. Rev. A **78**, 043416 (2008).
[31] D. A. Horner, T. N. Rescigno, and C. W. McCurdy, Phys. Rev. A **81**, 023410 (2010).
[32] A. Palacios, T. N. Rescigno, and C. W. McCurdy, Phys. Rev. A **79**, 033402 (2009).
[33] M. Førre, S. Selstø, and R. Nepstad, Phys. Rev. Lett. **105**, 163001 (2010).
[34] W.-C. Jiang, J.-Y. Shan, Q. Gong, and L.-Y. Peng, Phys. Rev. Lett. **115**, 153002 (2015).
[35] A. Liu and U. Thumm, Phys. Rev. Lett. **115**, 183002 (2015).
[36] X. Guan, K. Bartschat, and B. I. Schneider, Phys. Rev. A **77**, 043421 (2008).
[37] I. A. Ivanov and A. S. Kheifets, Phys. Rev. A **75**, 033411 (2007).
[38] R. Shakeshaft, Phys. Rev. A **76**, 063405 (2007).
[39] S. X. Hu, J. Colgan, and L. A. Collins, J. Phys. B **38**, L35 (2005).
[40] S. Selstø, X. Raynaud, A. S. Simonsen, and M. Førre, Phys. Rev. A **90**, 053412 (2014).
[41] L. A. A. Nikolopoulos and P. Lambropoulos, J. Phys. B **40**, 1347 (2007).
[42] C. Yu and L. B. Madsen, Phys. Rev. A **94**, 053424 (2016).
[43] P. Schlagheck, D. Ullmo, J. D. Urbina, K. Richter, and S. Tomsovic, Phys. Rev. Lett. **123**, 215302 (2019).
[44] W.-C. Jiang and J. Burgdörfer, Opt. Express **26**, 19921 (2018).
[45] O. I. Tolstikhin, Phys. Rev. A **77**, 032712 (2008).
[46] K. Toyota, O. I. Tolstikhin, T. Morishita, and S. Watanabe, Phys. Rev. A **76**, 043418 (2007).
[47] K. Toyota, O. I. Tolstikhin, T. Morishita, and S. Watanabe, Phys. Rev. A **78**, 033432 (2008).
[48] P. V. Demekhin and L. S. Cederbaum, Phys. Rev. Lett. **108**, 253001 (2012).
[49] P. V. Demekhin and L. S. Cederbaum, Phys. Rev. A **88**, 043414 (2013).

[50] A. N. Artemyev, A. D. Müller, D. Hochstuhl, L. S. Cederbaum, and P. V. Demekhin, Phys. Rev. A **93**, 043418 (2016).
[51] M. Baghery, U. Saalmann, and J. M. Rost, Phys. Rev. Lett. **118**, 143202 (2017).
[52] A. Palacios, T. N. Rescigno, and C. W. McCurdy, Phys. Rev. Lett. **103**, 253001 (2009).
[53] J. Feist, S. Nagele, C. Ticknor, B. I. Schneider, L. A. Collins, and J. Burgdörfer, Phys. Rev. Lett. **107**, 093005 (2011).
[54] V. Stooß, S. M. Cavaletto, S. Donsa, A. Blättermann, P. Birk, C. H. Keitel, I. Březinová, J. Burgdörfer, C. Ott, and T. Pfeifer, Phys. Rev. Lett. **121**, 173005 (2018).
[55] R. R. Freeman, P. H. Bucksbaum, H. Milchberg, S. Darack, D. Schumacher, and M. E. Geusic, Phys. Rev. Lett. **59**, 1092 (1987).
[56] J. G. Story, D. I. Duncan, and T. F. Gallagher, Phys. Rev. Lett. **70**, 3012 (1993).
[57] T. F. Gallagher, Phys. Rev. Lett. **61**, 2304 (1988).
[58] J. H. Eberly and K. C. Kulander, Science **262**, 1229 (1993).
[59] See Supplemental Material at http://link.aps.org/supplemental/10.1103/PhysRevLett.124.043203 for more details.
[60] T. N. Rescigno and C. W. McCurdy, Phys. Rev. A **62**, 032706 (2000).
[61] M. J. Rayson, Phys. Rev. E **76**, 026704 (2007).
[62] B. I. Schneider and L. A. Collins, J. Non-Cryst. Solids **351**, 1551 (2005).
[63] T. Park and J. Light, J. Chem. Phys. **85**, 5870 (1986).
[64] C. Leforestier, R. Bisseling, C. Cerjan, M. Feit, R. Friesner, A. Guldberg, A. Hammerich, G. Jolicard, W. Karrlein, H.-D. Meyer, N. Lipkin, O. Roncero, and R. Kosloff, J. Comput. Phys. **94**, 59 (1991).
[65] E. Cormier and P. Lambropoulos, J. Phys. B **29**, 1667 (1996).
[66] H. Muller, Laser Phys. **9**, 138 (1999).
[67] A. N. Grum-Grzhimailo, B. Abeln, K. Bartschat, D. Weflen, and T. Urness, Phys. Rev. A **81**, 043408 (2010).
[68] D. G. Arbó, J. E. Miraglia, M. S. Gravielle, K. Schiessl, E. Persson, and J. Burgdörfer, Phys. Rev. A **77**, 013401 (2008).
[69] M. Pont, N. R. Walet, and M. Gavrila, Phys. Rev. A **41**, 477 (1990).